optica

Surface plasmon assisted control of hot-electron relaxation time: supplementary material

SARVENAZ MEMARZADEH[1,2†], JONGBUM KIM[2,3,4†], YIGIT AYTAC[5], THOMAS E. MURPHY[1,2], AND JEREMY N. MUNDAY[1,2,3*]

[1]Department of Electrical and Computer Engineering, University of Maryland, College Park, Maryland 20742, USA
[2]Institute for Research in Electronics and Applied Physics , University of Maryland, College Park, Maryland 20742, USA
[3]Department of Electrical and Computer Engineering, University of California, Davis, California 95616, USA
[4]Nanophotonic Research Center, Korea Institute of Science and Technology (KIST), Seoul 02792, Korea
[5]Science Systems and Applications, Inc. Lanham, Maryland 20706, USA
[*]Corresponding author: jnmunday@ucdavis.edu

Published 27 May 2020

This document provides supplementary information to "Surface plasmon assisted control of hot-electron relaxation time," https://doi.org/10.1364/OPTICA.385959.

1. NUMERICAL AND EXPERIMENTAL MEASUREMENTS OF SURFACE PLASMON ABSORPTION

Absorption simulations and measurements for the sample using different incident wavelengths and surface plasmon coupling angles are illustrated in figure S1(a) and S1(b), respectively. As mentioned in the manuscript, the absorption in each case is computed from the transmission and reflectivity measurements. For the numerical calculation of absorption, we employ the transfer matrix method. For experimental measurements, at each wavelength the gold-coated prism is rotated using a motorized rotational stage. Surface plasmon coupling occurs under a specific angle, which suffices the momentum matching condition between the incident light and surface plasmons. This coupling results in maximum absorption of 85% over the range of the incident wavelengths. In order to have a fixed amount of absorbed power during our transient differential reflectivity measurements, we adjust the input power according to the expected absorption.

2. FREE ELECTRON MODEL

To calculate the changes in the permittivity function due to the intra-band optical pumping, we use a free electron model assuming a parabolic density of states. Starting with a constant value of the carrier density at room temperature, $N_e(T = 300K) = 5.049 * 10^{22}(1/cm^3)$, which is obtained from the ellipsometry fits, using the following equation [1]

$N_e(T = 300K) = \frac{1}{\pi^2}\int_0^\infty \frac{m_{T=300K}}{\hbar^2}\left(\frac{2m_{T=300K}E}{\hbar^2}\right)^{\frac{1}{2}} f_o(\mu_{T=300K}, T)dE$,

the chemical potential can be computed as $\mu_{T=300K} = 4.4526eV$. In the above equation, f_o is the Fermi-Dirac distribution and

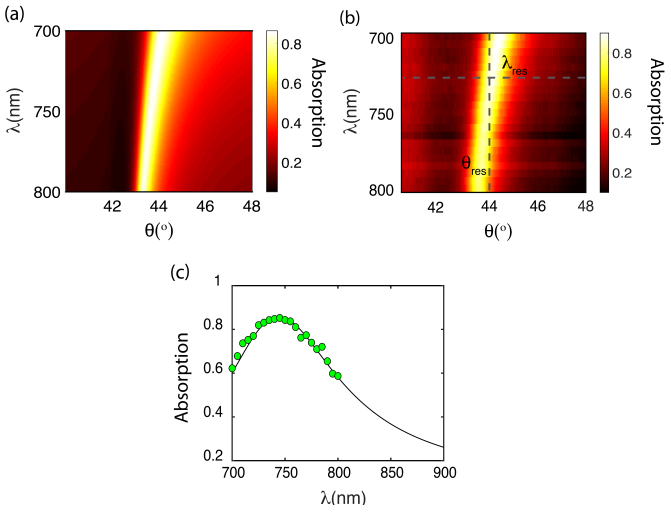

Fig. S1. (a) Simulation and (b) measurement absorption for the gold sample while coupling to the propagating surface plasmon for different incident wavelengths. In (c), the solid line (simulation) and dots (experiment) are extracted from the computed mesh plots in (a) and (b) at 745 nm resonance wavelength, respectively.

$m_{T=300K}$ is the electron mass at room temperature.
Under the assumption of a fixed chemical potential level and the same carrier density as for the intra-band optical pumping $(i.e. N_e(T) = N_e(T = 300K))$, we can further extract the effective electron mass at a higher temperature $m^*(T) = \frac{m(T)}{m_o}$ from [1]:

$N_e(T) = \frac{1}{\pi^2}\int_0^\infty \frac{m(T)}{\hbar^2}\left(\frac{2m(T)E}{\hbar^2}\right)^{\frac{1}{2}} f_o(\mu,T)dE.$

Finally, permittivity as a function of the electron temperature can be calculated in terms of the summation between the Drude term (w.r.t to the carrier density (N_e) and mobility (μ) as the fitting parameters) and Lorentz term according to [2]:

$\epsilon(\omega,T) = \epsilon_\infty + \frac{-\hbar^2 e^2 N_e \mu_n}{\epsilon_o(\mu_n m(T)+i q\hbar E)} + \sum_n \frac{A_n B_n En_n}{En_n^2 - E^2 - iE.B_n}$,

in which ϵ_∞ is the high-frequency dielectric constant, ϵ_0 is the vacuum dielectric constant, $\hbar$ is the reduced Planck's constant, e is the electron charge, μ is the carrier mobility, A is the amplitude of oscillation, En is the center energy, B is the broadening amplitude, and n is the number of oscillators. Here, the number of oscillators used in the Drude and Lorentz terms are 1 and 2, respectively. All the fitting parameters obtained from the ellipsometry measurement are listed in table S1.

Table S1. List of the ellipsometry parameters

Parameters	Values
A_1	2.0093
A_2	6.1582
B_1	0.6250 (eV)
B_2	2.8199 (eV)
En_1	2.9580 (eV)
En_2	4.1900 (eV)
μ_1	6.353 $\left(\frac{cm^2}{V.S}\right)$
ϵ_∞	3.1990

3. FITTING PROCEDURE & ERROR BAR CALCULATION

Best fits are selected based on the calculation of the Normalized Mean Square Error (NMSE) between the measured and calculated temperature data from the two-temperature model. Complete set of the fits for the on- and off-resonance wavelengths are shown in figures S2.

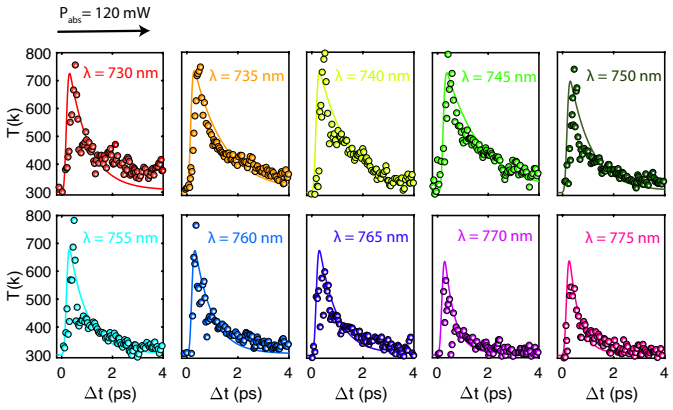

Fig. S2. Converted pump-probe data to the electron temperature for 10 different wavelengths with their corresponding best two-temperature model fits.

Error bars in the lifetime plot in the manuscript are obtained from the 95% confidence bounds calculation on the fitted coefficient (in our case lifetime). Error bars are computed according to the equation $c = p \pm t\sqrt{S}$. In this equation, p is the coefficient resulted from the fits. The variable t is computed using the inverse of the Student's t cumulative distribution (here corresponding to a 95% confidence bound), and S is the estimated covariance matrix from our measurements [3].

4. ELECTRIC FIELD PROFILES CALCULATION

To include the effect of surface plasmon coupling into our theoretical modeling, we modify the two-temperature model based on the absorbed power profiles $(P_{abs} = -\frac{1}{2}\omega||E|^2 Im(\epsilon))$ over the 10 different excitation wavelengths of our experiment. The absorbed power function is implemented for the profile simulation. For each incident wavelength, the input power is modified to keep the total absorbed power fixed (i.e. 120 mW) similar to our experiment. Figure S3 shows the results of the normalized electric field profiles over the range of the incident wavelengths. In Fig. S3, the black line corresponds to the electric field profile under no surface plasmon excitations ($\lambda = 745$ nm ,$\theta = 0^o$).

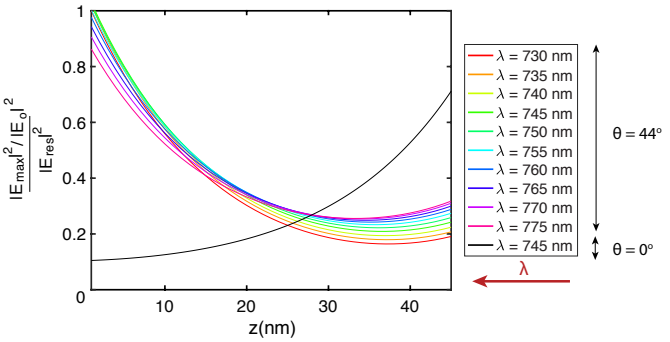

Fig. S3. Electric field profiles normalized by the intensity of the input field and the electric field at resonance wavelength of 745 nm. Profiles are computed from the FDTD simulation.

Each profile is then fitted with a double exponential equation in the form of $f(z) = a_1 e^{-z/b_1} + a_2 e^{(z-d)/b_2}$ over depth (z) to obtain the corresponding amplitude and decay length from each gold/air and gold/glass interface. Table S2 illustrates the results of the fitting parameters for the different incident wavelengths. Furthermore, z dependency of the hot-electrons lifetime and the maximum temperature at the resonance wavelength are shown in Fig. S4. This indicates a longer lifetime for the hot-electrons, which are closer to the gold interface. In this manuscript, the reported values of the relaxation times are computed after taking the average at various locations along the z direction.

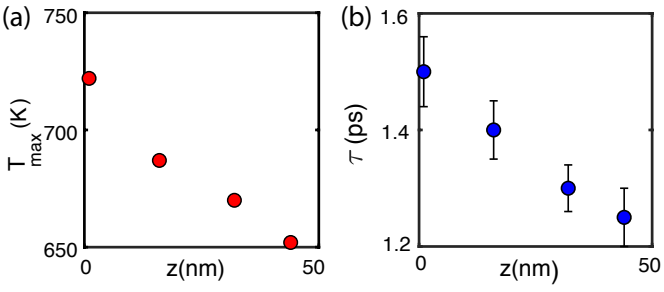

Fig. S4. (a) Maximum hot-electrons temperature and (b) relaxation time dependency along the sample thickness.

Table S2. Double exponential fitting parameters

Excitation $\lambda(nm)$	a_1	a_2	b_1(nm)	b_2(nm)
730	0.997	0.137	15.191	12.061
735	1.014	0.149	15.370	13.222
740	1.018	0.163	15.544	14.349
745	1.019	0.179	15.692	15.412
750	1.007	0.195	15.827	16.346
755	0.985	0.210	15.958	17.147
760	0.955	0.224	16.075	17.815
765	0.919	0.236	16.075	18.333
770	0.880	0.248	16.302	18.730
775	0.835	0.257	16.425	19.028

†These authors contributed equally.

REFERENCES

1. P. Guo, R. D. Schaller, J. B. Ketterson, and R. P. H. Chang, "Ultrafast switching of tunable infrared plasmons in indium tin oxide nanorod arrays with large absolute amplitude," Nat. Photonics **10**, 267–274 (2016).
2. J. A. Woollam Co, "CompleteEASE™ Data Analysis Manual," Tech. rep. (2004).
3. "Confidence and Prediction Bounds - MATLAB & Simulink," https://www.mathworks.com/help/curvefit/confidence-and-prediction-bounds.html.